Estuaries and Coasts
DOI 10.1007/s12237-014-9885-3

Quantifying the Residence Time and Flushing Characteristics of a Shallow, Back-Barrier Estuary: Application of Hydrodynamic and Particle Tracking Models

Zafer Defne · Neil K. Ganju

Received: 6 January 2014 / Revised: 4 September 2014 / Accepted: 4 September 2014

Abstract Estuarine residence time is a major driver of eutrophication and water quality. Barnegat Bay-Little Egg Harbor (BB-LEH), New Jersey, is a lagoonal back-barrier estuary that is subject to anthropogenic pressures including nutrient loading, eutrophication, and subsequent declines in water quality. A combination of hydrodynamic and particle tracking modeling was used to identify the mechanisms controlling flushing, residence time, and spatial variability of particle retention. The models demonstrated a pronounced northward subtidal flow from Little Egg Inlet in the south to Pt. Pleasant Canal in the north due to frictional effects in the inlets, leading to better flushing of the southern half of the estuary and particle retention in the northern estuary. Mean residence time for BB-LEH was 13 days but spatial variability was between ~0 and 30 days depending on the initial particle location. Mean residence time with tidal forcing alone was 24 days (spatial variability between ~0 and 50 days); the tides were relatively inefficient in flushing the northern end of the Bay. Scenarios with successive exclusion of physical processes from the models revealed that meteorological and remote offshore forcing were stronger drivers of exchange than riverine inflow. Investigations of water quality and eutrophication should take into account spatial variability in hydrodynamics and residence time in order to better quantify the roles of nutrient loading, production, and flushing.

Keywords Hydrodynamic modeling · Residence time · Particle tracking · Back-barrier estuaries · Eutrophication

Communicated by Charles Simenstad

Z. Defne (✉) · N. K. Ganju
U.S. Geological Survey, Woods Hole Coastal and Marine Science Center, Woods Hole, MA, USA
e-mail: zdefne@usgs.gov

Introduction

Estuarine eutrophication is a fundamental consequence of anthropogenic nutrient loading to the coast (Bricker et al. 1999). Typical symptoms include phytoplankton blooms (Paerl 1988), macroalgae proliferation (Valiela et al. 1997), seagrass dieback (Duarte 2002), and hypoxia (Rabalais and Turner 2001). Ultimately, eutrophication impairs the ecological function of estuaries in terms of biodiversity, habitat quality, and trophic structure. One primary physical control on eutrophication is estuarine flushing and ultimately residence time (González et al. 2008), which is defined as the time elapsed until a water parcel leaves a water body through one of its outlets. Estuaries with poor flushing and long residence times tend to retain nutrients within the system leading to high primary productivity rates (Lancelot and Billen 1984). Conversely, well-flushed estuaries are more resilient to nutrient loading due to reduced residence time and greater exchange with less impacted coastal waters.

Estuarine flushing and hydrodynamics are forced by tides, riverine flow, meteorological processes, and the resultant interactions with bathymetry and morphology. Tidal forcing results in bidirectional flows that can renew or mix water masses on tidal or spring-neap timescales.

Episodic riverine flows have the potential to completely flush an estuary and replace "old" water, while steady riverine flows can encourage a two-layer circulation that produces stratification and reductions in near-bed dissolved oxygen (Jassby and Van Nieuwenhuyse 2005). Wind can modify hydrodynamics via setup and wave-induced circulation (Csanady 1978), while barometric pressure fluctuations can induce changes in remote sea level that alter large scale pressure gradients and residual circulation (Wang 1979; Salas-Monreal and Valle-Levinson 2008; Walters and Gartner 1985). The combined effects of these forcings modify estuarine hydrodynamics and residence time on timescales ranging from hours to months.

Published online: 23 September 2014

Residence time is an integrative parameter that quantifies the renewal time for a given water parcel or water body. The calculation of residence time for particles in natural reservoirs was described by Bolin and Rodhe (1973); the concept was later extended and modified for coastal sea applications (Takeoka 1984; Zimmerman 1976). Although the terminology and precise definition tend to vary between studies, residence time and similar analyses are useful tools in estimating mixing and renewal of estuarine and coastal waters (Zhang et al. 2010). Particle tracking is one numerical technique for quantifying residence time in estuaries; multiple particles are released and tracked until transit out of the estuary. The change in total number of remaining particles in an estuary is often used as a measure of renewal rate of the estuarine water as well (Abdelrhman 2002; Brooks et al. 1999; Liu et al. 2004; Monsen et al. 2002). However, the residence time in an estuary is usually both spatially and temporally variable (Zhang et al. 2010), hence defining an average residence time for the entire estuary needs to be supplemented with the analysis of differential transport of particles within the domain.

In this study, we use a three-dimensional hydrodynamic model to identify the mechanisms controlling circulation and residence time in Barnegat Bay-Little Egg Harbor estuary (BB-LEH), New Jersey. BB-LEH has experienced several decades of declining water quality due to cultural eutrophication (Kennish et al. 2007; Kennish and Fertig 2012) yet the spatial and temporal variability in circulation and residence time is understudied. Guo and Lordi (2000) estimated an average residence time between 24 and 74 days (varying with season) based on measurements of velocity and salinity at Barnegat Inlet. Hydrodynamic modeling can elucidate the spatial variation of residence time and what mechanisms are responsible for flushing. We first detail the hydrodynamic setting of BB-LEH, followed by a description of the modeling system, skill assessment, particle tracking, and modeling scenarios. Then, the subtidal flow, flushing pattern, and residence time of the estuary are analyzed in terms of the individual influence of each inlet, delineated by forcing mechanisms in each scenario.

Site Description

The Barnegat Bay-Little Egg Harbor estuary spans 70 km along the Atlantic coast of New Jersey with a total surface area of ~280 km^2 (Fig. 1). Two inlets connect the estuary to the ocean; Little Egg Inlet at the southern end and Barnegat Inlet near the center. The Pt. Pleasant Canal connects the northern end of the estuary to the Manasquan River and ultimately to the ocean. Several rivers drain into the estuary, with the Toms River as the largest single point source of freshwater and nutrients. In general, the northern part of the estuary near the Toms River is considered the most eutrophic from an oxygen and primary productivity standpoint (Kennish et al. 2007; Kennish and Fertig 2012).

The southern end of the estuary begins with Little Egg Inlet, with a width of approximately 500 m and maximum depth of approximately 10 m. Moving northward, several deep channels wind through wide shoals, with vegetated marsh on the west side of the estuary and developed coastline on the east side. Barnegat Inlet is bordered by two jetties, with a mean width of 400 m and maximum depth approaching 15 m. Approaching Barnegat Inlet, a single north–south channel widens and several deep channels incise the flood tidal delta inside Barnegat Inlet. The northern half of the estuary is characterized by a 2- to 3-m-deep main channel, with wide shoals on the eastern back-barrier side. These shoals are colonized by eelgrass of varying density (Lathrop et al. 2006). The estuary gradually tapers to a narrow constriction before terminating at the Pt. Pleasant Canal. The canal is approximately 50 m wide and spans 3 km between Barnegat Bay and the Manasquan River. The terminus of the canal is 4 km from Manasquan Inlet and the Atlantic Ocean.

Tidal range outside the estuary is over 1 m, but attenuates rapidly landward. Between Barnegat Bay and Little Egg Inlet, the tide is attenuated gradually from 1 to 0.2 m. Due to the wide flood tidal shoal, Barnegat Inlet attenuates the tidal range to 0.2 m over a distance of 5 km (between Barnegat Inlet and Waretown; USGS NWIS 2012). Tidal velocities at the inlets exceed 2 m/s during spring tides, but also attenuate rapidly to 0.5 m/s or less throughout the estuary. Subtidal water levels and currents can be much larger during wind events or due to remote coastal forcing (Chant 2001).

Modeling and Analysis Methods

Domain

We used the Regional Ocean Modeling System (ROMS) (Shchepetkin and McWilliams 2005) within the COAWST modeling suite (Warner et al. 2010) for modeling the BB-LEH system. The computational domain included a part of Great Bay to the south and Manasquan Inlet to the north in addition to Barnegat Bay and Little Egg Harbor. The landward boundary on the west included several kilometers of river reaches and landward to streamflow gage locations wherever possible. The eastern boundary stretched offshore, approximately 2.5 km on the southeast and northeast corners and approximately 4 km at the middle of the eastern boundary. The computational grid consisted of 160 east–west and 800 north–south grid points with seven evenly distributed vertical layers. The computational cell sizes varied between 40 and 200 m in the horizontal with grid

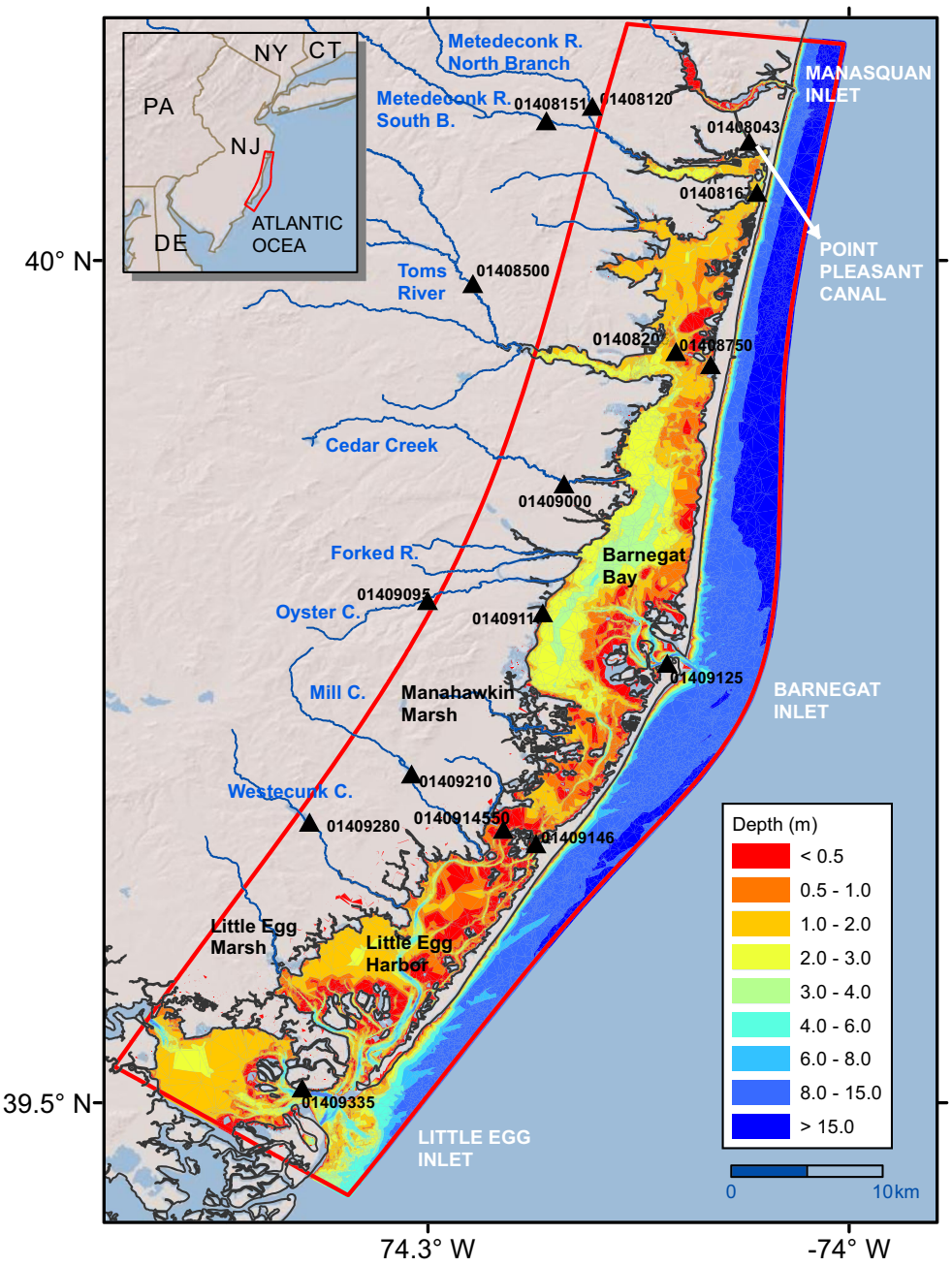

Fig. 1 Barnegat Bay-Little Egg Harbor (BB-LEH) estuary. *Red outline* is numerical model domain, *red dots* indicate measurement locations

refinement at the inlets and areas with detailed coastal features. Wetting and drying of intertidal areas were enabled (Warner et al. 2013), and a spatially uniform quadratic bottom roughness formulation was used in the simulation. After 5 days of model spin-up, the period between 1 March 2012 and 1 May 2012 was simulated with a computational time step of 5 s.

Bathymetry

The bathymetry of the model was based on the National Ocean Service Hydrographic Survey data (NOAA NOS 2012) and updated with recent bathymetric measurements (Miselis et al. 2012). The NOS data dates back to 1930s and does not represent the modern bathymetry or shoreline at certain locations. For example, the geometry of Barnegat Inlet was altered by construction of a sand dike and jetty realignment in the 1940s, which was not reflected in the NOS data set. At the time of this study, 65 % of the domain where water depth was larger than 1.5 m was updated with the new measurements. This included the navigational channel to the south of Pt. Pleasant Canal and the section between the Barnegat Inlet and the Toms River.

Model Forcing

The hydrodynamic model requires boundary forcing at landward and seaward ends, as well as the ocean–atmosphere interface. At the landward end (western boundary), we specified point sources of freshwater in accordance with USGS streamflow measurements at seven gages (USGS NWIS 2012; Table 1), and a radiation boundary condition that allows tidal energy to propagate landward. On the seaward end, tidal water level and velocity amplitudes from the ADCIRC tidal constituents' database for the North Atlantic (Mukai et al. 2002) were applied. These were supplemented by the subtidal water level and subtidal barotropic velocity from the ESPreSSO model, which covers the Mid-Atlantic Bight at 6 km resolution (Wilkin and Hunter 2013). At the ocean boundary, a combination of Chapman, Flather, and gradient boundary conditions were used. Salinity and temperature were also supplied by the ESPreSSO model. A radiation condition with nudging on a 6 h timescale for tracers allowed for the relaxation of the model solution relative to the forcing data, which prevented sharp gradients at the seaward boundary and subsequent oscillations in the solution. At the ocean–atmosphere interface, we applied meteorological forcing from North American Mesoscale Model (NCEP NAM 2012). The bulk flux parameterization routine was used with 3-h wind velocity, air pressure, long- and shortwave radiation, relative humidity, and rain inputs.

Calibration and Skill Assessment

The model was calibrated by changing the bottom roughness coefficient to attain the best agreement between the first 2 weeks post-spin-up model results and water level and tidal discharge measurements collected within BB-LEH by the U.S. Geological Survey (Table 2). A quadratic drag formulation with a drag coefficient of 0.0015 was used to define the bottom roughness for the entire domain throughout the duration of simulation. For calibration and skill assessment, the Brier Skill Score (Murphy and Epstein 1989) was used, where the skill of the model was given by

$$\mathrm{BSS} = \frac{\alpha - \beta - \gamma + \varepsilon}{1 + \varepsilon} \tag{1}$$

where BSS is the Brier skill score and

$$\alpha = r_{XY}^2, \beta = \left(r_{XY} - \frac{\sigma_Y}{\sigma_X}\right)^2, \gamma = \left(\frac{\langle Y\rangle - \langle X\rangle}{\sigma_X}\right)^2, \varepsilon = \left(\frac{\langle X\rangle}{\sigma_X}\right)^2 \tag{2}$$

where r is the correlation coefficient, σ is the standard deviation, ε is a normalization term, and X and Υ are the observed and modeled values, respectively. By definition, the Brier skill score (BSS) accounts for a phase error (α), an amplitude error (β), and a deviation (γ) from the mean value. The score is normalized by a term (ε) that depends on variations in the observed values. For a perfect skill, α=1 and β=γ=0. When the observed mean is used as the baseline prediction for skill, the BSS is equivalent to the Nash Sutcliffe Model Efficiency (Nash and Sutcliffe 1970). A skill score of 1.0 means a perfect match between the observed data and the model, zero means the model has no predictive skill beyond the mean observed value, and negative values indicate model has no predictive skill. For values between 0 and 1, the rating was assumed to be excellent for greater than 0.65, very good for 0.65–0.5, good for 0.5–0.2, and poor for less than 0.2 based on the related literature (Allen et al. 2007; Ralston et al. 2010; Sutherland et al. 2004). Additionally, Root-Mean-Square-Error (RMSE) was used as a supplementary measure of model skill.

Particle Tracking

The Lagrangian TRANSport model (LTRANS) (North et al. 2011) was used for particle tracking. LTRANS runs offline with hydrodynamic model output for velocity, density, and

Table 1 Streamflow measurements used as input for BB-LEH model

Station no	Station name	Latitude	Longitude
01408120	North Branch Metedeconk River near Lakewood	40° 05′ 30″	74° 09′ 09″
01408151	South Branch Metedeconk River near Lakewood	40° 04′ 59″	74° 10′ 47″
01408500	Toms River	39° 59′ 11	74° 13′ 24″
01409000	Cedar Creek at Lanoka Harbor	39° 52′ 03″	74° 10′ 09″
01409095	Oyster Creek near Brookville	39° 47′ 54″	74° 15′ 01″
01409210	Mill Creek at Manahawkin	39° 41′ 43″	74° 15′ 35″
01409280	Westecunk Creek at Stafford Forge	39° 40′ 00″	74° 19′ 13″

Table 2 Comparison of BB-LEH model results for water level (WL) and tidal discharge magnitude (Q) with the measurements (*RMSE* RMS Error, *BSS* Skill Score)

Station no	Station name	Latitude	Longitude	Parameter	Max	Mean	RMSE	BSS	Skill
01408167	Mantoloking	40° 02′ 26″	74° 03′ 17″	WL (m)	0.61[a]	0.17[a]	0.10	0.55	Very good
01408750	Seaside Heights	39° 56′ 18″	74° 04′ 56″	WL (m)	0.53[a]	0.23[a]	0.09	0.57	Very good
01408205	Rt 37 bridge	39° 56′ 46″	74° 06′ 09″	WL (m)	0.42[a]	0.22[a]	0.09	0.53	Very good
01409110	Waretown	39° 47′ 28″	74° 10′ 55″	WL (m)	0.50[a]	0.21[a]	0.09	0.50	Good
01409147	Barnegat Light	39° 45′ 40″	74° 06′ 29″	WL (m)	1.05[a]	0.69[a]	0.10	0.86	Excellent
01409146	East Thorofare	39° 39′ 14″	74° 11′ 09″	WL (m)	0.70[a]	0.47[a]	0.13	0.59	Very good
01409335	Little Egg Inlet	39° 30′ 32″	74° 19′ 29″	WL (m)	1.38[a]	0.89[a]	0.15	0.81	Excellent
01408043	Pt Pleasant Canal	40° 04′ 15″	74° 03′ 34″	Q (m^3/s)	378	191	53	0.93	Excellent
01409125	Barnegat Light	39° 45′ 40″	74° 06′ 29″	Q (m^3/s)	3707	1494	567	0.88	Excellent
0140914550	Rt 72 bridge	39° 39′ 48″	74° 12′ 25″	Q (m^3/s)	616	235	192	0.50	Good

[a] Maximum and mean values display tidal range in case of water level measurements

vertical diffusivity to calculate particle paths. Particles were defined as neutrally buoyant and passive with a random displacement substituting for vertical turbulent motion. They were released in a uniform fashion: one particle at the central node of each nine neighboring grid nodes (approximately 30 to 200 m apart, but less than 100 m on average) inside the BB-LEH estuary. Preliminary tests with bottom, mid-depth, and surface releases showed no significant difference in ensemble statistics; half of the particles after an hour of release were found to be evenly distributed between the top and bottom halves of the water column. Hence, particles were released near the surface at each scenario for simplicity. A total of 79,632 particles (3318 particles on every hour of the first day) were released, and they were not tracked once they left the estuarine system.

The flushing accomplished by each inlet of the BB-LEH estuary was quantified by calculating the percentage of particles removed through each inlet by the end of the simulation period. The percentages correspond to the ratio of the number of cases in which a particle released at a certain location leaves the estuary to the total number of cases. The residence time for each particle was defined as days elapsed upon exit after the initial release.

We compared different methods to determine a system-wide mean residence time for the BB-LEH estuary. First, a mean residence time was calculated by ensemble averaging individual particle residence times in the domain over all releases

$$T_{re} = \frac{1}{R}\frac{1}{N}\sum_{j=1}^{R}\sum_{i=1}^{N}(t_r)_{ij} \tag{3}$$

where T_{re} is the mean residence time based on ensemble averaging, R=24 is the total number of releases, N=3318 is the total number of particles, and $(t_r)_{ij}$ is the residence time, for the i^{th} particle in j^{th} release.

In some cases, a portion of the particles may remain in the domain at the end of the simulation period. This causes the ensemble averaging to yield a smaller mean residence time than a case where the simulation is run long enough for all of the particles to leave the domain. A fit function, on the other hand, is helpful to infer the general trend in data from finite number of data points. Therefore, a single-exponential decay function was fit to the change in total number of particles in the domain

$$\frac{N(t)}{N_0} = Ce^{-kt} \tag{4}$$

where N_0 is the initial number of particles in the domain, $N(t)$ is the number of particles at time t, and C and k are coefficients of the decay function.

In systems with varying timescales of flushing, a double-exponential decay function provides a more conforming fit, with a higher correlation coefficient than a single-exponential decay function (Choi and Lee 2004; Neumann 2007; Periáñez et al. 2013). A double-exponential decay function was also used

$$\frac{N(t)}{N_0} = \alpha e^{-k_1 t} + (1-\alpha)e^{-k_2 t} \tag{5}$$

where α, k_1, and k_2 are characteristic coefficients of a two-staged system; with an initial stage of rapid drop in number of particles followed by a slower decay stage. The mean residence times were calculated respectively for single and double decay functions by

$$T_{rs} = \frac{1}{k} \tag{6}$$

$$T_{rd} = \frac{\alpha}{k_1} + \frac{1-\alpha}{k_2} \tag{7}$$

following Choi and Lee (2004).

Another set of metrics used was based on the particle travel distances and included the spatial distribution of the average path length, the average net displacement, and the average tortuosity or relative meandering of the particle path. The average path length was calculated as the average of the total absolute distance traveled by a particle at each time step in all of the releases and given by

$$L = \frac{1}{R}\sum_{j=1}^{R}\sum_{i=1}^{m}\sqrt{\left(x_j^{i+1}-x_j^{i}\right)^2+\left(y_j^{i+1}-y_j^{i}\right)^2} \tag{8}$$

where L is the average path length, m is the total number of time steps, and x and y are coordinates of a particle at a given time step. The average net displacement is the average Euclidian distance traveled and was defined as the average of the difference between the initial and final coordinates of a particle for all releases

$$d = \frac{1}{R}\sum_{j=1}^{R}\left|\left(x_j^{m},y_j^{m}\right)-\left(x_j^{1},y_j^{1}\right)\right| \tag{9}$$

Finally, we utilized tortuosity, which can be described in terms of the ratio between the path length and the net displacement, as an indicator for the characteristics of particle transport from a location. The ratio of average net displacement to the average path length was subtracted from 1 so that a straight line of transport would have a value of 0 and a looped transport would have a value of 1

$$\tau = 1-\frac{d}{L} \tag{10}$$

where τ is the tortuosity. A nine-point averaging scheme was applied to travel distance and tortuosity maps in order to reduce the irregularities.

Scenarios

In order to assess the relative influences of different forcing mechanisms on the residence time in BB-LEH, each forcing was sequentially added to the model. These scenarios were:

1. Scenario T (Tidal forcing only):
   Water level and velocity constituents from the ADCIRC tidal database were applied at the open boundaries.
2. Scenario TB (Tidal and supplemental boundary forcing):
   Tidally averaged water level and current forcing from the EsPreSSO model were added to the tidal forcing at the open boundaries. EsPreSSO time series for temperature and salinity were used with a radiation type open boundary condition.
3. Scenario TBR (Tidal, boundary, and riverine forcing):
   Streamflow data from the measurements were incorporated along with the forcing from scenario TB.
4. Scenario TBRM (Tidal, boundary, riverine, and meteorological forcing):
   Wind speed and direction, surface air pressure, air temperature, relative humidity, rain, and solar radiation fluxes over the computational domain were incorporated along with the forcing from Scenario TBR.

Modeling Results and Discussion

Skill Assessment

BB-LEH model skill score ranged from very good to excellent in predicting the water levels and tidal discharges according to the BSS rating (Table 2). Temperature and salinity skill scores were classified as excellent and good, respectively (Table 3). The model predicted water levels at Barnegat and Little Egg Inlets with BSSs of 0.86 and 0.81 and RMS errors of 0.10 and 0.15 m, respectively. The skill was lower within the bay, likely due to insufficient representation of modern bathymetry. Tidal range was significantly attenuated in the bay, especially west and north of Barnegat Inlet (with mean tidal range around 0.20 m) as compared to the southern part of the bay (0.47 m at East Thorofare) in agreement with the findings of Chant (2001). The model predicted tidal discharges at Pt. Pleasant Canal and the Barnegat Inlet with skill scores of 0.93 and 0.88, respectively, while no measurement data were available to compare the results at Little Egg Inlet. Based on the measurements at Mantoloking station, temperature was modeled with a skill of 0.84 while salinity skill was markedly lower at 0.39 (Table 3). The salinity time-series showed large fluctuations up to 6 psu at the tidal timescale. It is likely that a salt front in northern Barnegat Bay may be advecting southward from Pt. Pleasant Canal on flood tides (e.g., from Manasquan Inlet). The model does not resolve this potential salt front, perhaps due to poor representation of mixing and advection processes or insufficient model resolution in this narrow constriction. The subtidal variation in salinity and temperature at Mantoloking Bridge was reproduced with a BSS=0.48 and 0.87, respectively. On the other hand, the skill score for tidally averaged water levels was always lower (BSS≅ 0.3) even when the BSS for unfiltered values were excellent. This is a result of BSS formulation, the RMS error gets penalized more as the amplitude of the tidally averaged water levels is smaller and the variance of filtered measurement data closes to zero.

Table 3 Comparison of BB-LEH model results for temperature (T) and salinity (S) results with the measurements at the Mantoloking station (*RMSE* RMS Error, *BSS* Skill Score)

Station no	Station name	Latitude	Longitude	Parameter	Max	Min	RMSE	BSS	Skill
01408167	Route 528 bridge	40° 02′ 26″	74° 03′ 17″	T (deg C)	19.3	8.5	1.0	0.84	Excellent
				S (psu)	28.6	19.0	2.2	0.39	Good

Tidal and Subtidal Hydrodynamics

Tidal discharge at Barnegat and Little Egg Inlets was an order of magnitude larger than the tidal discharge than the Pt. Pleasant Canal. The modeled average maximum flood discharges for Little Egg Inlet, Barnegat Inlet, and Pt. Pleasant Canal during the simulation periods were 2501, 2412, and 254 m^3/s, respectively. For ebb tides, they were 1894, 2111, and 246 m^3/s. The tidal range reduced rapidly from 1 to 0.2 m inland of Barnegat Inlet and kept decreasing to the north, whereas a more gradual attenuation was observed from Little Egg Inlet (1 m) to the south of Barnegat Inlet (0.2 m). Delay in tidal propagation through the inlets increased from zero at Little Egg Inlet to 3 to 4 h a few kilometers to the south of Barnegat Inlet, back to zero at Barnegat Inlet, and then gradually up to 5 h to the south of Pt. Pleasant Canal. The tidal propagation was 1 h faster during high tide than during low tide.

The subtidal hydrodynamics in BB-LEH were heavily influenced by remote coastal forcing. This effect was included in the model by incorporating the tidally averaged signals from the larger scale ESPreSSO model at the open boundaries. The model results were improved significantly by this method as seen in the subtidal water level time series and to a certain extent in the tracer time series within the estuary. A low-pass filter with a cutoff frequency of 1/33 h (Flagg et al. 1976) was used to remove the tidal signals. Modeled time series from selected locations and the maps of residual flow were analyzed to explain the spatiotemporal nature of the low frequency signal in the bay. The model indicated a northward residual circulation from Little Egg Inlet to Barnegat Inlet and Pt. Pleasant Canal during the simulation period (Fig. 2). The residual inflow at Little Egg Inlet (64 m^3/s) and the tributaries (10 m^3/s) was compensated with the outflow at Barnegat Inlet (56 m^3/s) and Pt. Pleasant Canal (17 m^3/s), and the rate of increase in the bay volume over the simulation period (1 m^3/s). In order to determine the major driving force behind the residual circulation, we analyzed the residual flows in all four scenarios (Table 4). When forced only with tides, the pattern of the subtidal circulation was the same, with some change in magnitudes; the inflow at the Little Egg Inlet (50 m^3/s) was compensated with the outflow at the Barnegat Inlet (34 m^3/s) and Pt. Pleasant Canal (15 m^3/s), and the rate of change in the bay volume (1 m^3/s). On average, approximately 75 % of the residual flow observed at each inlet in TBRM was already present when the model was forced with tides only. This indicates that nonlinear hydrodynamic interactions and tidal rectification (interaction of tidal flow with bathymetry) are significant drivers of the subtidal flow in the bay. The addition of boundary and forcing in scenario TB increased the absolute value of the residual flows by 5 % on average. In scenario TBR, a relatively larger increase was observed in outflow at Barnegat Inlet (14 %) compared to Little Egg Inlet (−5 %) and Pt. Pleasant Canal (~0 %). When meteorological forcing was included with scenario TBRM, an average increase on the order of 20 % was observed in the residual current. Chant (2001) proposed that subtidal water levels and currents in BB-LEH were mainly controlled by coastal sea levels and to a lesser extent by local winds. Our modeling results also demonstrate the relative dominance of coastal sea levels over local winds.

Momentum balance analyses elucidate the spatiotemporal variation in hydrodynamic mechanisms that generate the resultant flows (Ganju et al. 2011). The depth-averaged momentum balance is given by

$$\frac{\partial u_i}{\partial t} + u_{ji}\frac{\partial u_i}{\partial x_j} - f u_j = -\frac{1}{\rho}\frac{\partial P}{\partial x_i} + \frac{1}{\rho h}\frac{\partial (h\tau_{ij})}{\partial x_j} - \frac{\tau_i^b}{\rho h} + \frac{\tau_i^s}{\rho h} \qquad (11)$$

where u is the depth-averaged velocity, f is the Coriolis parameter, P is the pressure, ρ is the water density, h is the water depth, τ_{ij} is the stress tensor, τ_i^b is the bottom stress, and τ_i^s is the surface stress. The first term is local acceleration, the second term is horizontal advection, the third term is Coriolis force, the fourth term is pressure gradient, the fifth term is horizontal viscosity, the sixth term is bottom stress, and the seventh term is surface stress.

We examined the time series and the spatial variation of the residual momentum terms in BB-LEH to determine the relative importance of each term. For brevity, we present here figures from along-estuary momentum balance analysis only and note any differences from the cross-estuary balance when necessary. Along the Little Egg Inlet, horizontal advection was largely balanced by the pressure gradient with a smaller contribution from bottom stress (Fig. 3a, b) while the remaining terms were an order of magnitude smaller (Fig. 4a). The contribution from the bottom stress and pressure gradient terms increased when the inlet bathymetry was shallower. In

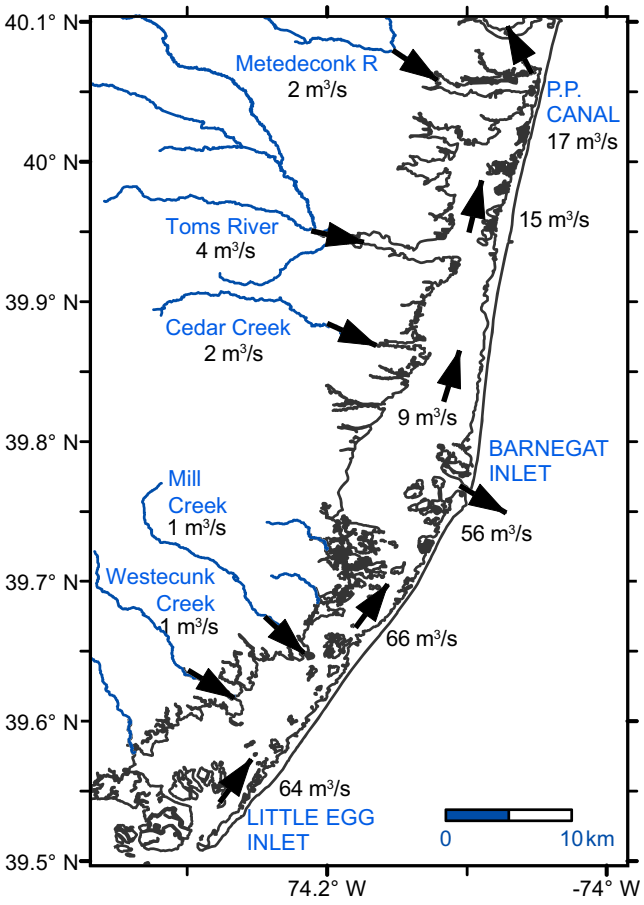

Fig. 2 Laterally and depth-averaged residual circulation in BB-LEH over the March–May 2012 simulation period

both along and cross-estuary directions, the surface stress due to winds was strongest where depth was less than 1 m; this term dominated the momentum balance with an opposing pressure gradient and bottom stress at depths shallower than 0.5 m during strong wind events (Figs. 3c, d and 4b). Winds with speeds greater than 8 m/s blew mostly from south-southwest and northwest in the estuary during the simulation period (Fig. 5). The residual surface stress during the simulation period was towards the northeast and was maximized over the shallow flats between Little Egg Harbor and Barnegat Bay (between 39.57 and 39.74 °N). Comparison of water level time series between scenarios TBR and TBRM revealed that a 10 m/s sustained wind event from the south could cause a 0.25 m additional increase in the water level near the Pt. Pleasant Canal (or decrease with wind from the north). A much larger range of additional variation in water level was observed near Pt. Pleasant Canal (0.55 m) than at Little Egg Inlet (0.08 m) when these two scenarios were compared, highlighting the unique response of BB-LEH to changes in wind stress along the estuary.

We compared the tidally averaged water level and current time series at various cross-sections against the tidally averaged along-estuary wind velocity to clarify this further. The correlation was quantified using a Pearson correlation coefficient (R) at each location. With the positive north and positive up sign convention, a positive correlation factor meant an increase in the water level (or increase in the current flow to north) with increased south winds (vice versa in case of north winds). South winds caused an additional increase in water level on the northern estuary and additional decrease on the south with increasing magnitudes towards both ends. Additionally, the correlation was highest closer to Pt. Pleasant Canal ($R>0.8$) and reduced towards Barnegat Inlet ($R\cong0.5$), changed sign somewhere around the Manahawkin Marsh ($R\cong 0.0$) and increased with an opposite sign towards Little Egg Inlet ($R\cong-0.5$) implying a subtidal oscillation of the water surface around an axis across Manahawkin Marsh with respect to the along-estuary winds. The maximum range of oscillations was 0.03 m. The change in subtidal current followed the same trend with southern along-estuary winds contributing positively to northward currents. However, the correlation was weaker closer to the inlets and higher at the axis of the subtidal water surface oscillation. The maximum range was on the order of 0.02 m/s. Barnegat Inlet was investigated for a correlation between cross-estuary winds and subtidal water level and currents to find a weak correlation during the simulation period ($R<0.5$).

Spatial Pattern of Flushing

Over 75 % of the domain, more than 90 % of particles were flushed out of BB-LEH at the end of the 2-month simulation period (Fig. 6a). The percent removal was 100 % over 18 % of the domain, meaning that particles released over 18 % of the domain exited it in all of the 24 releases. The percent removal reduced to approximately 80 % for particles released between Tice's Shoal and Kettle Creek, 70 % for particles released in Toms River, and 60 % for particles released near Little Egg Marsh. In some of the sheltered and shallow areas along the coastline (Mordecai, Long Beach, Sedge Islands, and Manahawkin Marsh) and landward ends of small channels, the removal percentage ranged from 0 to 60 %, indicating poor flushing.

Pt. Pleasant Canal flushed 100 % of the particles from a 13 km^2 area in the north, extending 6 km south from the canal to the north of Kettle Creek and Long Island Cove. The canal also removed 50 % of the particles 15 km to the south across the mouth of the Toms River, and up to 40 % of the particles in the seaward end of the Toms River (Fig. 6b). Barnegat Inlet removed particles from 224 km^2 of the estuary, stretching from the Toms River to 4 km inshore of Little Egg Inlet (Fig. 6c). Barnegat Inlet also removed up to 40 % of the particles originating in the Toms River. However, the most

Table 4 Mass balance between residual current at the inlets, total river inflow, and change in bay volume for each scenario during the simulation period

Scenario	Little Egg Inlet (m^3/s)	Barnegat Inlet (m^3/s)	Pt Pleasant Canal (m^3/s)	River inflow (m^3/s)	Rate of change in volume (m^3/s)	Average absolute change with each additional forcing (%)
TBRM	64	−56	−17	10	−1	20
TBR	49	−45	−14	10	0	6
TB	52	−37	−14	0	−1	5
T	50	−34	−15	0	−1	76

Average percent change with each additional forcing is calculated with respect to the TBRM scenario, e.g., in case of additional boundary forcing in TB: Little Egg Inlet (52–50)/64=3 %; Barnegat Inlet (37–34)/56=5 %; Pt. Pleasant Canal (14–15)/17=−6 %; Average absolute change (3+5+|−6|)/3=5 %

efficient flushing (80 % removal) occurred in a 92 km^2 area south of Barnegat Inlet, as a result of the northward residual flow from Little Egg Inlet. All of the particles within a 5 km^2 area, extending 4 km into the bay, were removed through Little Egg Inlet in all 24 releases (Fig. 6d). Although Barnegat and Little Egg Inlets had comparable tidal discharge, the total number of particles that exit the estuary through Little Egg Inlet was substantially smaller, due to the dominant subtidal transport to the north.

Residence Time by Scenario

Tides alone removed a majority of particles from BB-LEH, but other forcings tended to incrementally enhance flushing (Table 5, Fig. 7). The mean residence time in Scenario T (tides only) was 23.9 days and reduced to 13.0 days in the full-forcing Scenario TBRM. From a percent removal perspective, 85 % of all of the particles in BB-LEH were removed by the end of the simulation in Scenario T and increased to 89, 90, and 93 % with the addition of boundary, riverine, and meteorological forcing, respectively. In Scenario TBRM, 77 % removal was observed when mean residence time was reached at T_{rd}=13.0 day (Fig. 7b). By that time, 59, 66, and 67 % of the particles were removed in Scenarios T, TB, and TBR. Overall, the increase in the removal rate due to addition of boundary and meteorological forcings was comparable, but the effect of riverine forcing was substantially smaller.

The spatial variation of residence time in each scenario was quantified by mapping residence time based on the initial starting location of the particle.

Scenario T When forced with tides only (Scenario T), most of the particles originating in Toms River and Barnegat Bay between 39.86 and 39.95 °N remained in the bay at the end of the simulation period (Fig. 8a). Residence times for 44 % of the particles released in Barnegat Bay and 32 % of the particles released in Little Egg Harbor were larger than 28 days in this case. The largest residence times were observed in Kettle

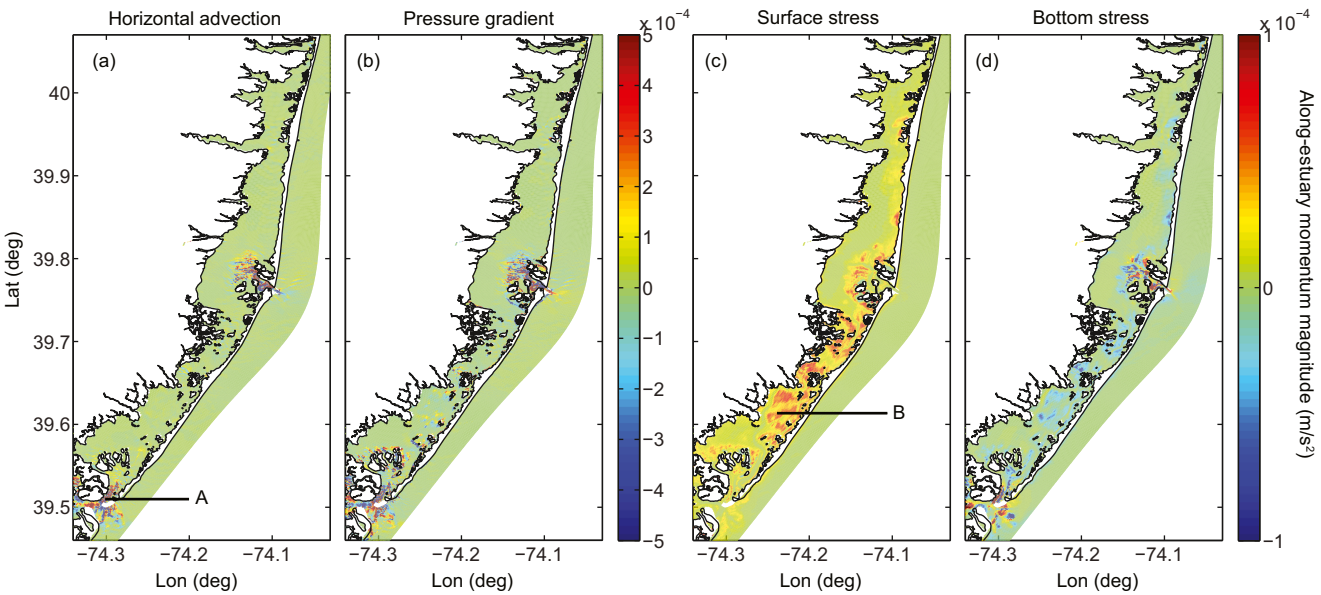

Fig. 3 Spatial maps of time-averaged terms in the along-estuary momentum balance: **a** horizontal advection, **b** pressure gradient, **c** surface stress, and **d** bottom stress

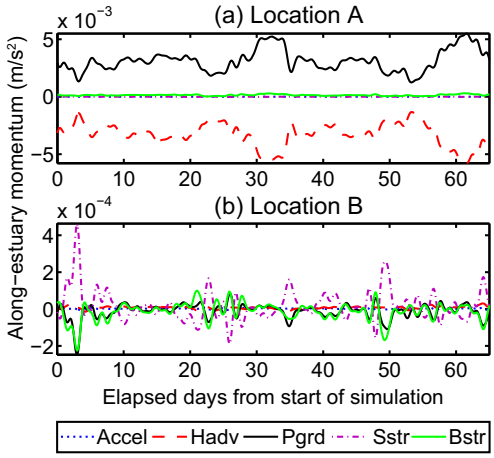

Fig. 4 Time-series of terms in the along-estuary momentum balance from **a** Little Egg Inlet and **b** a shoal in Little Egg Harbor

Creek and near Little Egg Marsh, and Mordecai Island on the south.

Scenario TB When the remote coastal forcing was introduced as a subtidal forcing at the open boundary, the largest reduction in residence time was in Little Egg Harbor (14–21 days). Similarly, in Barnegat Bay, a similar decrease was seen in the largest residence times observed south of Toms River. The decrease in residence time was less than 1 day for the particles originating near Pt. Pleasant Canal. Inclusion of the boundary forcing increased the subtidal flow magnitude in the bay by 5 to 8 % depending on cross-section. Additionally, maximum discharge through the inlets was also increased resulting in a longer local tidal excursion. Hence, the reduction in the residence times was mainly associated with a larger northward flow through Little Egg Inlet and enhanced flushing through

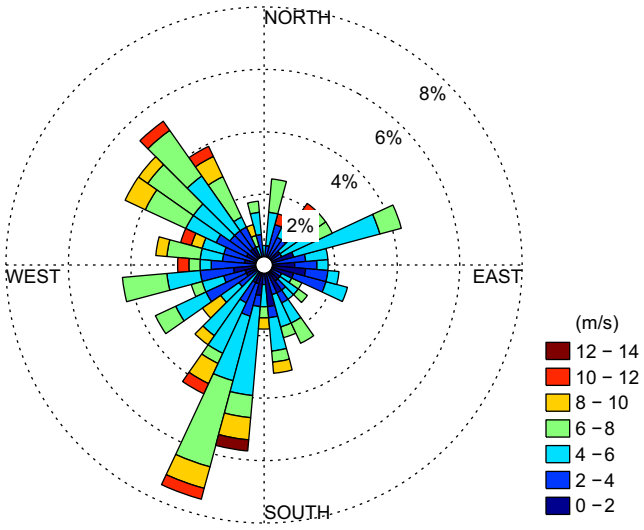

Fig. 5 Winds over the domain predicted by the NAM model during the simulation period, March and April 2012

Barnegat Inlet. Patches of increased residence time on the order of few days were noticeable in Toms River, Silver Bay, and Kettle Creek. This anomaly is likely due to the random nature of particles with only a slight variation between the simulations.

Scenario TBR Inclusion of the riverine flow in the model caused up to a 14 days reduction in the residence time upstream of major tributaries (Cedar Creek, Toms and Metedeconk Rivers; Fig. 8c). Residence time between the Toms and Forked Rivers was also reduced by 7 days on average in this scenario. Riverine inflow increased the residual outflow at Barnegat Inlet, whereas it decreased the residual inflow at Little Egg Inlet. This uneven contribution to the residual circulation might be the reason for the irregularly distributed increases in residence time (up to 7 days) that were observed at Kettle Creek and Silver Creek in the north and to the west of Westecunk Creek in the south.

Scenario TBRM The inclusion of meteorological forcing reduced the residence time in the least energetic part of the estuary (between 39.90 and 40.02 °N) by up to 28 days. Maximum reduction was observed on the eastern half of this area, over the shallow waters with depth less than 1 m. The decrease in Kettle Creek, Silver Bay, and downstream Toms River was generally limited to 14 days. Similarly, the residence time in the majority of the least energetic area in the south (i.e., the northern half of Little Egg Harbor and the southwest corner) was reduced nearly by 14 days in this scenario. The drop along the Manahawkin Marsh shore was on the order of 10 day. On the other hand, in this scenario, it took up to 14 days longer than the TBR scenario for particles released over Tice's Shoal on the north of Sedge Islands (in an area about 17 km^2) to leave the estuary. Animations of particle motion showed that the particles released in this area exited the estuary through Barnegat Inlet within the first 14 days of simulation in Scenario TBR. Wind events during the first 14 days of simulation prevented transport of these particles towards Barnegat Inlet in Scenario TBRM. The difference (TBRM–TBR) in the subtidal water level across the mouth of Toms River for the two scenarios showed a wind setup that was strongly correlated with the south winds (Fig. 9). Because the subtidal current over the submerged shoals is governed by winds in BB-LEH, strong south winds increased the northward transport over Tice's Shoal during this period. The meteorological events during the simulation period seemed to be a larger driver of flushing than the rivers, as they caused a larger drop in the residence time and a larger change in the subtidal flow (an average increase in subtidal flow of ~20 % compared to ~5 % increase from rivers). The long fetch in the N-S direction in BB-LEH allows for sustained momentum transfer over the air–sea interface during periods of N-S winds.

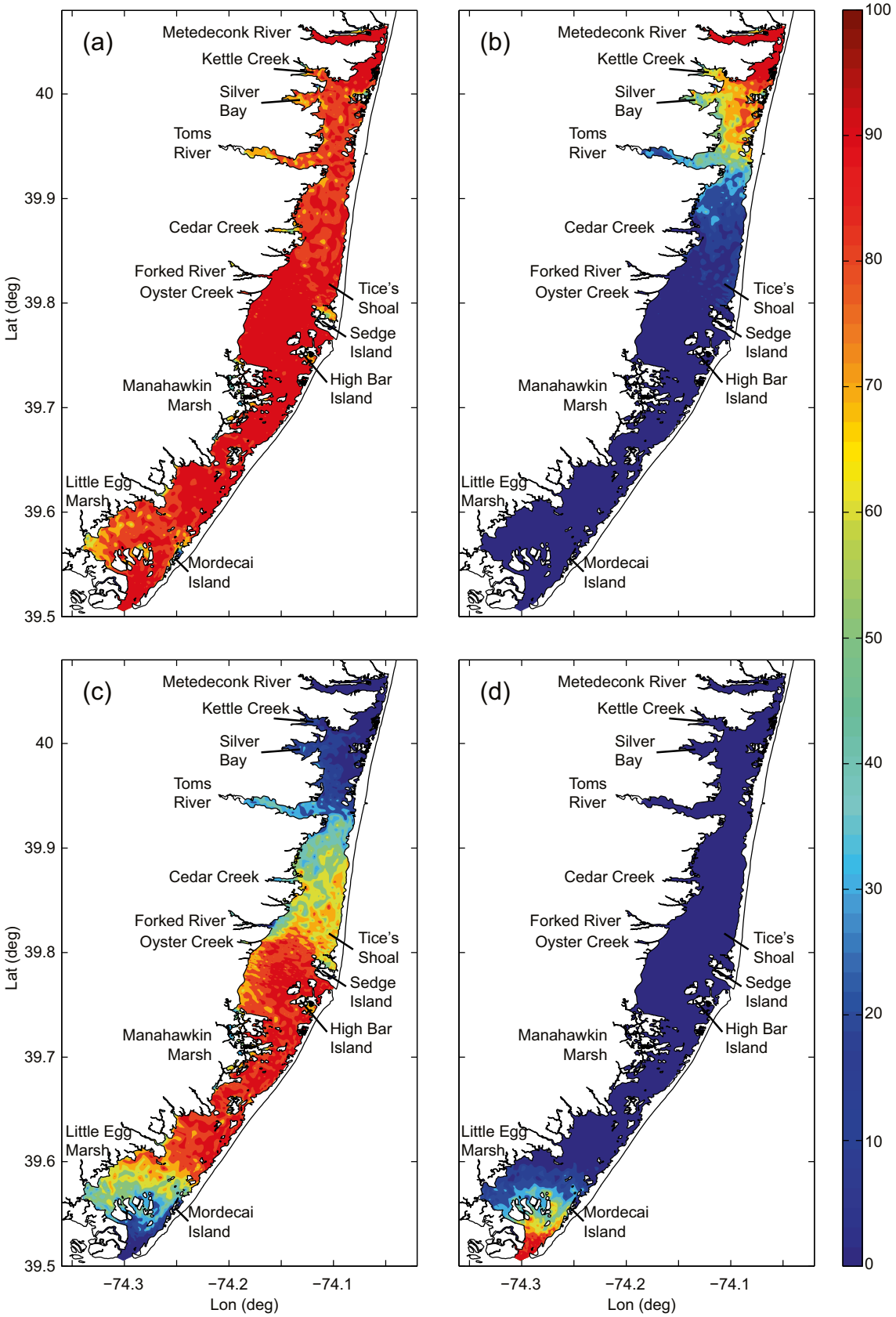

Fig. 6 Spatial flushing characteristics in terms of the percentage of particles removed through **a** all inlets, **b** Pt. Pleasant Canal only, **c** Barnegat Inlet only, and **d** Little Egg inlet only at the end of simulation period

Table 5 Mean residence time calculated by ensemble averaging of individual residence times (T_{re}), by fitting single (T_{rs}), and double-exponential decay functions (T_{rd}) to change in number of particles in BB-LEH domain in each different forcing scenario (*T* Tidal, *B* Boundary, *R* River, *M* Meteorological forcing)

	T_{re} (days)	T_{rs} (days)	T_{rd} (days)	α	k_1	k_2
T	19.2	19.0	23.9	0.440	0.378	0.025
TB	16.2	14.4	19.0	0.533	0.360	0.027
TBR	15.4	13.6	17.4	0.511	0.410	0.030
TBRM	11.5	8.8	13.0	0.700	0.277	0.029

α, k_1, and k_2 are coefficients of double-exponential decay function

The ensemble average of the particle path length in BB-LEH was ~290 km. The average for the particles released in the poorly flushed areas of Barnegat Bay and Little Egg Harbor was, respectively, 41 % (≅410 km) and 34 % (≅390 km) larger than the ensemble average (Fig. 10a). Although the average path length for particles in each of these areas was equal, the average net displacement varied substantially. Compared to the ensemble average of net displacement by all particles in BB-LEH (≅18 km), the averages for poorly flushing areas were 31 % shorter (≅12 km) for the area between Silver Bay and Toms River, but 100 % longer (≅36 km) for the Little Egg Marsh (Fig. 10b). The dissimilarity was due to the stronger northward transport due to larger subtidal current in Little Egg Harbor. Most of the particles (>70 %) drifted to the north by subtidal flow left the estuary through Barnegat Inlet while the remaining (<30 %) traveled further into the northern Barnegat Bay.

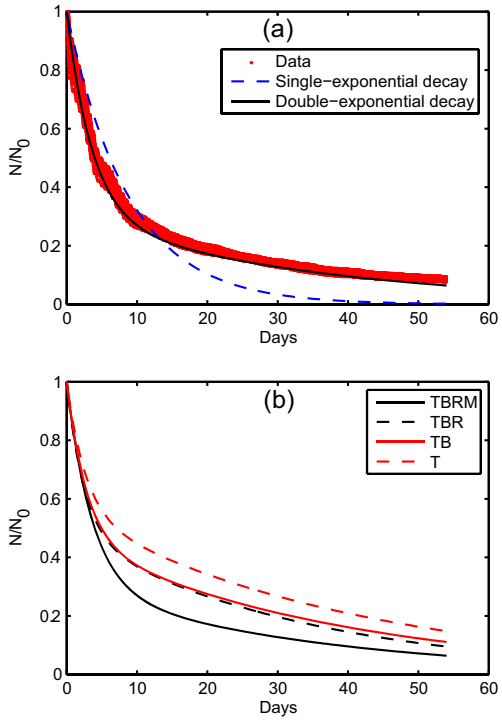

Fig. 7 **a** Change in fraction of particles that remain in BB-LEH domain during scenario TBRM. **b** Double-exponential decay function fits for all for scenarios under combination of following forces; *T* tides, *B* Boundary, *R* River, *M* Meteorological

Due to tidal motion, the minimum tortuosity was never less than 0.6, meaning that the average path length was always over 2.5 times larger than the net displacement. Minimum values of tortuosity were observed near Little Egg Inlet and Pt. Pleasant, where particles exited the domain within the first few days of the simulation. In comparison, tortuosity at Barnegat Inlet was larger due to the more complex geometry of the inlet, a meandering main channel and broad flood tide shoals that connect to relatively much deeper water on the west. The mean tortuosity for the entire estuary was 0.91. Particles released at the southwest corner of Little Egg Harbor traveled long paths, but the tortuosity of the transport was close to the mean of the estuary. On the other hand, for the particles released between Toms River and Kettle Creek in Barnegat Bay that traveled long paths the tortuosity was the highest, a unique characteristics of the particle transport in the BB-LEH estuary.

Spatial Gradients in Residence Time and Water-Quality

Kennish et al. (2007, 2012) highlighted the eutrophication of BB-LEH and the role of watershed development, nutrient loading, and primary production. Northern Barnegat Bay and the Toms River have higher primary production and lower water-quality due to these processes; our results also suggest that reduced flushing may be exacerbating eutrophication. In all four scenarios, particles deployed in the northern bay between Kettle and Cedar Creeks (~65 km^2 including upstream Toms River and Cedar Creek) had the longest residence time. Kennish et al. (2007) also suggest a temporal variation in eutrophication with lowest water quality occurring during the summer when nutrient loading and photoperiod are maximized. This is also a period of less energetic wind forcing; our results show that wind stress is a major factor in residual flows over the shallows and reduces residence time on a basin-wide scale. Additionally, Little Egg Marsh in the south also had poor flushing compared to the rest of the bay due to a location sheltered from winds and tides, and relatively deeper water. Prior studies (Olsen and Mahoney 2001) have identified high phytoplankton concentrations in this area, possibly enhanced by relatively poor flushing. This study suggests that spatial variations in hydrodynamics and flushing are substantial in back-barrier estuaries and should be considered in water-quality studies to properly gauge the relative influence of nutrient loading, production, and flushing.

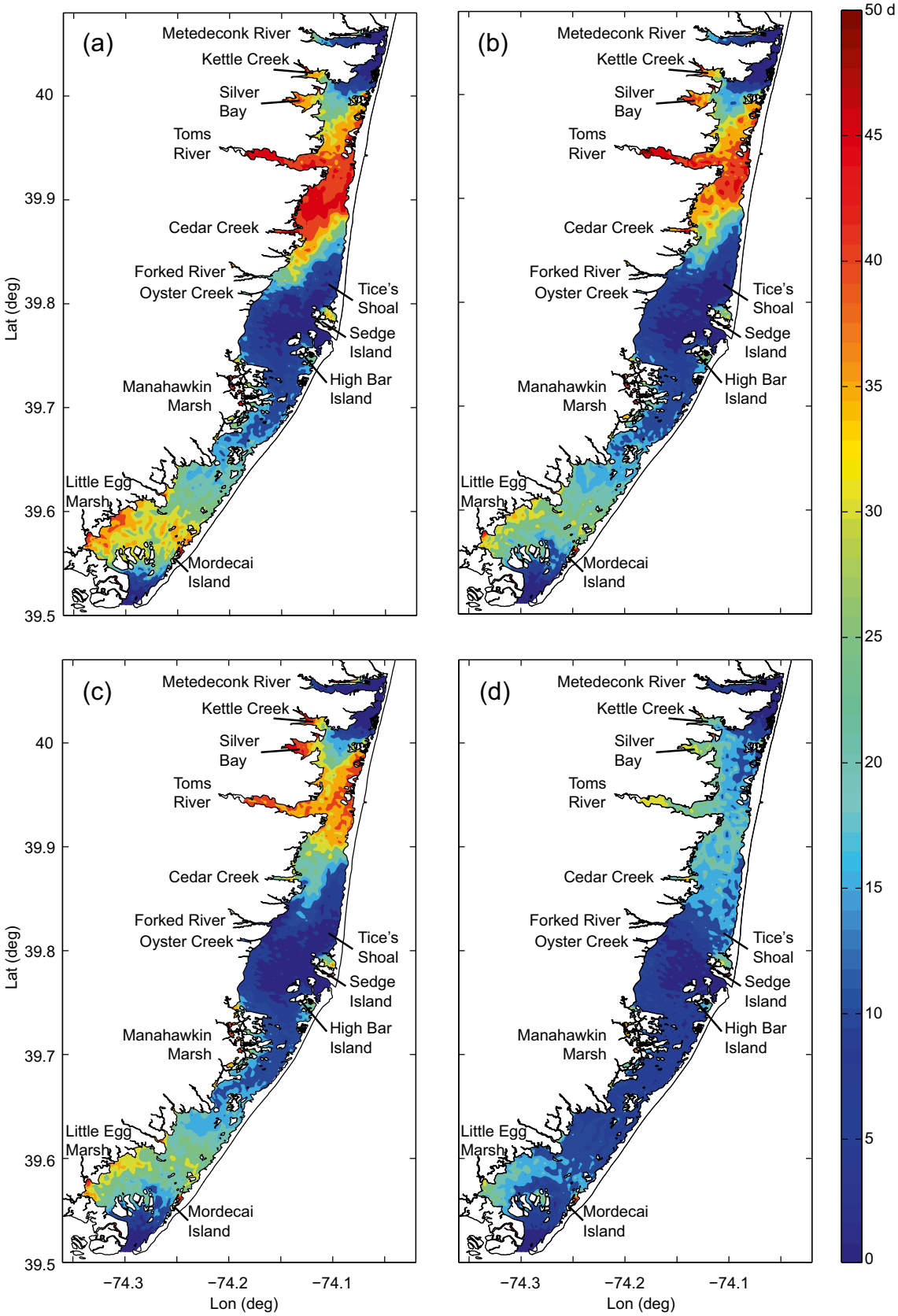

Fig. 8 Residence times in days for **a** scenario T, only tidal forcing; **b** scenario TB, combined offshore hydrodynamic forcing; **c** scenario TBR, streamflow with combined hydrodynamic forcing; and **d** scenario TBRM, full suite with meteorological forcing

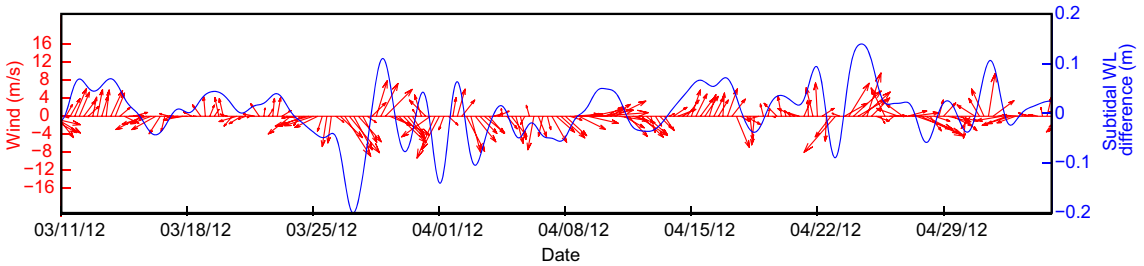

Fig. 9 Difference in subtidal water level between two scenarios (TBRM-TBR; *blue*) and wind time series (*red arrows*, up indicates N direction) for Tice's Shoal for the same period. South and East winds prevail during the first weeks of simulation (3/11–3/24)

Conclusions

Hydrodynamic modeling of Barnegat Bay-Little Egg Harbor (BB-LEH) demonstrated that subtidal motion in the estuary is a major contributor in determining the mode of flushing of estuarine water and the spatial distribution of residence times in the domain. A northward residual flow resulted in enhanced flushing of the southern half of the estuary between Little Egg and Barnegat Inlets. Flushing from the part of the estuary between Barnegat Inlet and the Pt. Pleasant Canal was relatively poor due to weak tidal and subtidal flow. The relative change in residual flow between four scenarios scenario suggested that about 75 % of the forcing behind the residual circulation is from tides due to tidal rectification as a result of the friction and the geometry of the estuary, followed by the local winds (20 %), rivers (5 %), and the remote forcing (5 %). Comparison of the full-forcing scenario to a scenario with no meteorological forcing revealed a strong correlation between the along-estuary winds and the subtidal motion in the bay. Evaluation of the tidally averaged horizontal momentum balance terms shows that over shallow flats, surface stress due to wind was the main driver behind the subtidal flow and was mostly balanced by the pressure gradient and the bottom stress. On the other hand, near the inlets horizontal advection was an order of magnitude larger and mainly balanced by the pressure gradient with a smaller contribution from bottom stress.

The rate of particle removal under different forcing mechanisms indicated that the meteorological events and the remote coastal forcing were stronger flushing mechanisms than river inflow. The mean residence time for BB-LEH was calculated by three different methods; ensemble averaging of the

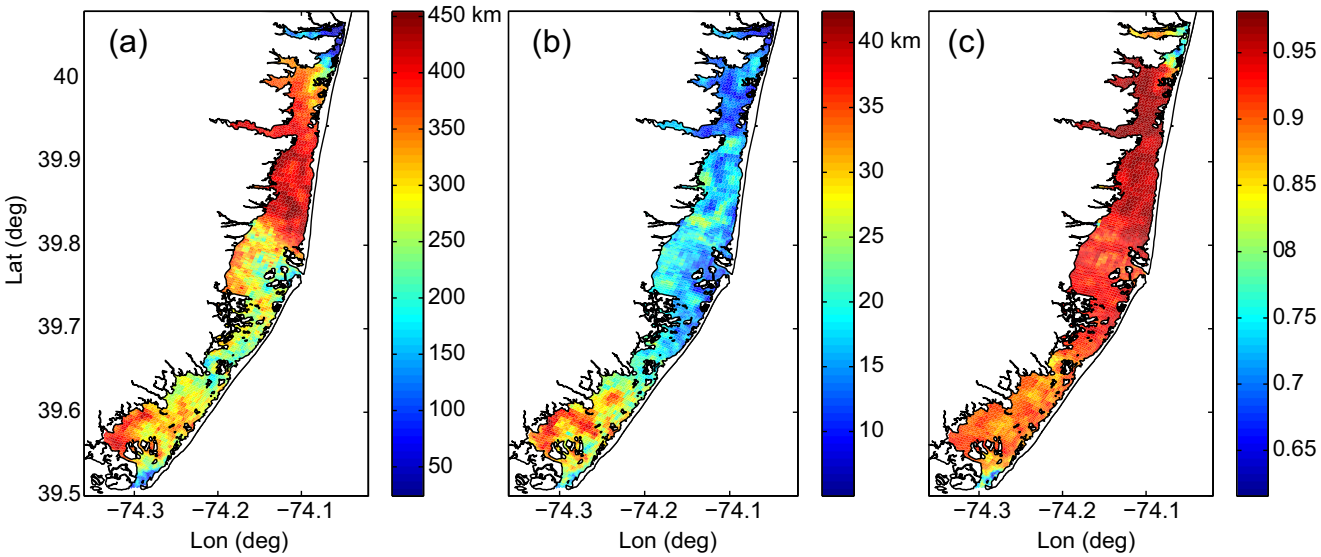

Fig. 10 **a** Average path traveled, **b** average net displacement (Euclidean distance), and **c** tortuosity for each particle release location in the BB-LEH estuary

local residence times, fitting a single-exponential decay function to the change of number of particles in the bay after the initial release and by fitting a double-exponential decay function yielding 11.5, 8.8, and 13 days, respectively. The value of mean residence time relied on the method used suggesting that when comparing mean residence time between different systems identical methods should be used if none of the methods is superior to the others. We preferred using a double-exponential decay function, because a fit function provides means for extrapolation and in case of the BB-LEH estuary mean residence time estimated by the double-exponential decay function was a statistically better fit than a single-exponential decay.

Residence time maps differentiated between energetic and idle regions in the estuary in terms of exchange of water, yielding spatial gradients in residence time as large as 20 days over a few kilometers. The particle tracking analysis also revealed regions with different particle transport characteristics in the BB-LEH estuary. The region between Kettle Creek and Toms River on the north had the largest tortuosity, meaning that the transport path length to net displacement ratio was the largest in this area. Particles released in the southwest of the Little Egg Harbor also traveled very long paths but their tortuosity was closer to the mean of the estuary. Particles released near Little Egg Inlet and Pt. Pleasant Canal had the lowest tortuosity values and were the first to leave the estuary within the first few days of the simulation.

In this paper, we analyzed the findings from the hydrodynamic and particle tracking models in terms of residence time, which does not provide any information on the destination for particle transport explicitly. The present study can be extended with a connectivity analysis in order to identify common sources and destinations in the domain and systematically quantify the connectivity between them. Nevertheless, investigations of water quality and eutrophication should take into account spatial variability in hydrodynamics and residence time in order to better quantify the roles of nutrient loading, production, and flushing.

Acknowledgments Funding was provided by the New Jersey Department of Environmental Protection and the Coastal and Marine Geology Program of the U.S. Geological Survey. Assistance was provided by John Warner, Jennifer Miselis, and Brian Andrews. Hydrologic data collection by the New Jersey Water Science Center of the U.S. Geological Survey was invaluable to this study, and we thank Anthony Navoy and Robert Nicholson for their assistance.

References

Abdelrhman, M.A. 2002. Modeling how a hurricane barrier in New Bedford Harbor, Massachusetts, affects the hydrodynamics and residence times. *Estuaries* 25(2): 177–196.

Allen, J., P. Somerfield, and F. Gilbert. 2007. Quantifying uncertainty in high-resolution coupled hydrodynamic-ecosystem models. *Journal of Marine Systems* 64(1–4): 3–14. doi:10.1016/j.jmarsys.2006.02.010.

Bolin, B., and H. Rodhe. 1973. A note on the concepts of age distribution and transit time in natural reservoirs. *Tellus* 25(1): 58–62.

Bricker, S.B., C.G. Clement, D.E. Pirhalla, S.P. Orlando, and D.R. Farrow. 1999. *National estuarine eutrophication assessment: Effects of nutrient enrichment in the nation's estuaries*. Silver Spring: NOAA, National Ocean Service, Special Projects Office and the National Centers for Coastal Ocean Science.

Brooks, D.A., M.W. Baca, and Y.T. Lo. 1999. Tidal circulation and residence time in a macrotidal estuary: Cobscook Bay, Maine. *Estuarine, Coastal and Shelf Science* 49: 647–665.

Chant, R.J. 2001. Tidal and subtidal motion in a shallow bar-built multiple inlet/Bay system. *Journal of Coastal Research* 32(Special Issue): 102–114.

Choi, K.W., and J.H.W. Lee. 2004. Numerical determination of flushing time for stratified water bodies. *Journal of Marine Systems* 50(3–4): 263–281.

Csanady, G.T. 1978. The arrested topographic wave 1. *Journal of Physical Oceanography* 8: 47–62.

Duarte, C.M. 2002. The future of seagrass meadows. *Environmental Conservation* 29: 2–206.

Flagg, C.N., J.A. Vermersch, and R.C. Beardsley. 1976. 1974 MIT New England shelf dynamics experiment (March 1974). Data Report, Part II: the moored array, MIT Report 76–1.

Ganju, N.K., S.J. Lentz, A.R. Kirincich, and J.T. Farrar. 2011. Complex mean circulation over the inner shelf south of Martha's Vineyard revealed by observations and a high-resolution model. *Journal of Geophysical Research* 116, C10036. doi:10.1029/2011JC007035.

González, F.U.T., J.A. Herrera-Silveira, and M.L. Aguirre-Macedo. 2008. Water quality variability and eutrophic trends in karstic tropical coastal lagoons of the Yucatán Peninsula. *Estuarine, Coastal and Shelf Science* 76(2): 418–430.

Guo, Q., and G.P. Lordi. 2000. Method for quantifying freshwater input and flushing time in estuaries. *Journal of Environmental Engineering* 126: 675–683.

Jassby, A., and E.E Van Nieuwenhuyse. 2005. Low dissolved oxygen in an estuarine channel (San Joaquin River, California): mechanisms and models based on long-term time series. *San Francisco Estuary and Watershed Science* 3(2).

Kennish, M.J., and B. Fertig. 2012. Application and assessment of a nutrient pollution indicator using eelgrass (Zostera marina L.) in Barnegat Bay–Little Egg Harbor estuary, New Jersey. *Aquatic Botany* 96(1): 23–30.

Kennish, M.J., S.B. Bricker, W.C. Dennison, P.M. Glibert, R.J. Livingston, K.A. Moore, R.T. Noble, H.W. Paerl, J.M. Ramstack, S. Seitzinger, D.A. Tomasko, and I. Valiela. 2007. Barnegat Bay-Little Egg Harbor Estuary: case study of a highly eutrophic coastal bay system. *Ecological Applications* 17: 3–16.

Lancelot, C., and G. Billen. 1984. Activity of heterotrophic bacteria and its coupling to primary production during the spring phytoplankton bloom in the Southern Bight of the North Sea. *Limnology and Oceanography* 29: 721–730.

Lathrop, R.G., P. Montesano, and S. Haag. 2006. A multi-scale segmentation approach to mapping seagrass habitats using airborne digital camera imagery. *Photogrammetric Engineering and Remote Sensing* 72: 665–675.

Liu, Z., H. Wei, G. Liu, and J. Zhang. 2004. Simulation of water exchange in Jiaozhou Bay by average residence time approach. *Estuarine, Coastal and Shelf Science* 61(1): 25–35.

Miselis J., B. Andrews., R. Baker, W. Danforth, V. DePaul, Z. Defne, L. Feinson, N. Ganju, J. Gibs, R.E. Hickman, A. Lopez, A. Navoy, R. Nicholson, T. Reilly, R. Reiser, F. Spitz, A. Watson, C. Wieben, and T. Wilson. 2012. Characterizing physical, chemical, and biological conditions and processes in the Barnegat Bay-Little Egg Harbor

Estuary, New Jersey. 2012 Barnegat Bay Researchers Workshop, Bordentown Township, NJ.

Monsen, N.E., J.E. Cloern, L.V. Lucas, and S.G. Monismith. 2002. A comment on the use of flushing time, residence time, and age as transport time scales. *Limnology and Oceanography* 47(5): 1545–1553.

Mukai A.Y., J.J. Westerink, R.A. Luettich Jr., and D. Mark. 2002. Eastcoast 2001: A tidal constituent database for the western North Atlantic, Gulf of Mexico and Caribbean Sea. US Army Engineer Research and Development Center, Coastal and Hydraulics Laboratory, Technical Report, ERDC/CHL TR-02-24.

Murphy, A.H., and E.S. Epstein. 1989. Skill scores and correlation coefficients in model verification. *Monthly Weather Review* 117: 572–581.

Nash, J.E., and J.V. Sutcliffe. 1970. River flow forecasting through conceptual models: part 1. A discussion of principles. *Journal of Hydrology* 10(3): 282–290.

NCEP NAM. 2012. NAM-12 North America, NOAA Operational Model Archive and Distribution System, http://nomads.ncep.noaa.gov/. Accessed 2012.

Neumann, T. 2007. The fate of river-borne nitrogen in the Baltic Sea—an example for the River Oder. *Estuarine, Coastal and Shelf Science* 73(1–2): 1–7.

NOAA NOS. 2012. National Ocean Service Hydrographic Survey data, National Oceanic and Atmospheric Administration, http://www.ngdc.noaa.gov/mgg/bathymetry/hydro.html. Accessed 2012.

North, E.W., E.E. Adams, S. Schlag, C.R. Sherwood, S. Socolofsky, and R. He. 2011. Simulating oil droplet dispersal from the Deepwater Horizon spill with a Lagrangian approach. *AGU Book Series: Monitoring and Modeling the Deepwater Horizon Oil Spill: A Record Breaking Enterprise* 195: 217–226.

Olsen, P.S., and J.B. Mahoney. 2001. Phytoplankton in the Barnegat Bay-Little Egg Harbor estuarine system: Species composition and picoplankton bloom development. *Journal of Coastal Research, SI* 32: 115–143.

Paerl, H.W. 1988. Nuisance phytoplankton blooms in coastal, estuarine, and inland waters. *Limnology and Oceanography* 33: 823–847.

Periáñez, R., M. Casas-Ruíz, and J.P. Bolívar. 2013. Tidal circulation, sediment and pollutant transport in Cádiz Bay (SW Spain): a modelling study. *Ocean Engineering* 69: 60–69.

Rabalais, N.N., and R.E. Turner. 2001. Hypoxia in the northern Gulf of Mexico: Description, causes, and change. *Coastal and Estuarine Studies* 58: 1–36.

Ralston, D.K., W.R. Geyer, and J.A. Lerczak. 2010. Structure, variability, and salt flux in a strongly forced salt wedge estuary. *Journal of Geophysical Research* 115, C06005. doi:10.1029/2009JC005806.

Salas-Monreal, D., and A. Valle-Levinson. 2008. Sea-level slopes and volume fluxes produced by atmospheric forcing in estuaries: Chesapeake Bay Case study. *Journal of Coastal Research* 24(2A): 208–217.

Shchepetkin, A.F., and J.C. McWilliams. 2005. The Regional Ocean Modeling System: a split-explicit, free-surface, topography following coordinates ocean model. *Ocean Modelling* 9: 347–404.

Sutherland, J., A.H. Peet, and R.L. Soulsby. 2004. Evaluating the performance of morphological models. *Coastal Engineering* 51(8–9): 917–939.

Takeoka, H. 1984. Fundamental concepts of exchange and transport time scales in a coastal sea. *Continental Shelf Research* 3(3): 311–326.

USGS NWIS. 2012. National Water Information System, US Geological Survey. http://waterdata.usgs.gov/nwis. Accessed 2012.

Valiela, I., J. Mcclelland, J. Hauxwell, P.J. Behr, D. Hersh, and K. Foreman. 1997. Macroalgal blooms in shallow estuaries: controls and ecophysiological and ecosystem consequences. *Limnology and Oceanography* 42: 1105–1118.

Walters, R.A., and J.W. Gartner. 1985. Subtidal sea level and current variations in the Northern Reach of San Francisco Bay. *Estuarine, Coastal and Shelf Science* 21: 17–32.

Wang, D.P. 1979. Subtidal sea level variations in the Chesapeake Bay and relations to atmospheric forcing. *Journal of Physical Oceanography* 9: 413–421.

Warner, J.C., B. Armstrong, R. He, and J.B. Zambon. 2010. Development of a Coupled Ocean–Atmosphere–Wave–Sediment Transport (COAWST) modeling system. *Ocean Modeling* 35: 230–244.

Warner, J.C., Z. Defne, K. Haas, and H.G. Arango. 2013. A wetting and drying scheme for ROMS. *Computers & Geosciences* 58: 54–61.

Wilkin, J.L., and E.J. Hunter. 2013. An assessment of the skill of real-time models of Mid-Atlantic Bight continental shelf circulation. *Journal of Geophysical Research Oceans* 118(6): 2919–2933 doi:10.1002/jgrc.20223.

Zhang, W.G., J.L. Wilkin, and O.M.E. Schofield. 2010. Simulation of water age and residence time in New York Bight. *Journal of Physical Oceanography* 40: 965–982.

Zimmerman, J. 1976. Mixing and flushing of tidal embayments in the western dutch Wadden sea. Part I: distribution of salinity and calculation of mixing time scales. *Netherlands Journal of Sea Research* 10(2): 149–191.